A&A 475, 775–784 (2007)
DOI: 10.1051/0004-6361:20077191

Astronomy & Astrophysics

INTEGRAL/IBIS all-sky survey in hard X-rays⋆,⋆⋆

R. Krivonos[1,2], M. Revnivtsev[1,2], A. Lutovinov[2,1], S. Sazonov[1,2], E. Churazov[1,2], and R. Sunyaev[1,2]

[1] Max-Planck-Institute für Astrophysik, Karl-Schwarzschild-Str. 1, 85740 Garching bei München, Germany
e-mail: krivonos@mpa-garching.mpg.de
[2] Space Research Institute, Russian Academy of Sciences, Profsoyuznaya 84/32, 117997 Moscow, Russia

Received 29 January 2007 / Accepted 27 July 2007

ABSTRACT

We present results of an all-sky hard X-ray survey based on almost four years of observations with the IBIS telescope onboard the INTEGRAL observatory. The dead time-corrected exposure of the survey is ∼33 Ms. Approximately 12% and 80% of the sky has been covered to limiting fluxes lower than 1 and 5 mCrab, respectively. Our catalog of detected sources includes 403 objects, 316 of which exceed a 5σ detection threshold on the time-averaged map of the sky, and the rest were detected in various subsamples of exposures. Among the identified sources, 219 are Galactic (90 low-mass X-ray binaries, 76 high-mass X-ray binaries, 21 cataclysmic variables, 6 coronally active stars, and other types) and 137 are extragalactic, including 130 active galactic nuclei (AGNs) and 3 galaxy clusters. We derived number-flux functions of AGNs and Galactic sources. The $\log N$–$\log S$ relation of non-blazar AGNs is based on 68 sources located at Galactic latitudes $|b| > 5^\circ$, where the survey is characterized by high identification completeness, with fluxes higher than $S_{\rm lim} = 1.1 \times 10^{-11}$ erg s^{-1} cm^{-2} (∼0.8 mCrab) in the 17−60 keV energy band. The cumulative AGN number-flux function can be described by a power law with a slope of 1.62 ± 0.15 and normalization of $(5.7 \pm 0.7) \times 10^{-3}$ sources per deg^2 at fluxes $>1.43 \times 10^{-11}$ erg s^{-1} cm^{-2} (>1 mCrab). Those AGNs with fluxes higher than $S_{\rm lim}$ make up ∼1% of the cosmic X-ray background at 17−60 keV. We present evidence of strong inhomogeneity in the spatial distribution of nearby ($\lesssim$70 Mpc) AGNs, which reflects the large-scale structure in the local Universe.

Key words. surveys – X-rays: general – Galaxy: general – galaxies: Seyfert – cosmology: large-scale structure of Universe

1. Introduction

The INTEGRAL observatory (Winkler et al. 2003) has been successfully operating in orbit since its launch in 2002. Due to the high sensitivity and relatively good angular resolution of its instruments, in particular the coded-mask telescope IBIS (Ubertini et al. 2003), surveying the sky in hard X-rays is one of the primary goals of INTEGRAL. A number of papers have reported results of deep observations of relatively compact regions of the sky (e.g Revnivtsev et al. 2003a; Molkov et al. 2004; Krivonos et al. 2005a; Revnivtsev et al. 2006) and of systematic searches for sources over very large sky areas (e.g., Bird et al. 2006, 2007; Bazzano et al. 2006). However, until recently it was difficult to use INTEGRAL data for source population studies, in particular extragalactic ones, because the coverage of the sky remained substantially incomplete. Therefore, in 2005−2006 we performed dedicated observations of the previously unobserved regions of the sky and thereby completed the most sensitive all-sky survey ever in hard X-rays. In this paper, we present a catalog of sources detected during the all-sky survey (Sect. 4), discuss the number-flux relations of Galactic and extragalactic hard X-ray sources (Sect. 5), and investigate the spatial distribution of local AGNs (Sect. 6).

2. Survey coverage and sensitivity

The present survey is based on observations performed during the first four years of the INTEGRAL mission. We used data from the ISGRI detector of the IBIS telescope, which is well-suited to carrying out imaging surveys in hard X-rays. The coded-mask telescope IBIS provides a wide field of view of $28^\circ \times 28^\circ$ ($9^\circ \times 9^\circ$ fully coded) and moderate angular resolution of $12'$. The localization accuracy of $<2-3'$ is sufficiently good for searches of soft X-ray and optical counterparts and subsequent optical identification of newly discovered hard X-ray sources.

We used all the public and proprietary data available to us. The observations were performed during spacecraft revolutions from 25 (end of December 2002) to 463 (June 2006). Especialy important, our data set includes the special series of thirteen 200 ks-long extragalactic pointings (PI Churazov), which allowed us to complete the survey of the entire sky. Figure 2 shows the fraction of the sky covered by the survey as a function of the limiting flux for source detection with at least 5σ significance. Approximately 12% and 80% of the sky is covered down to 1 and 5 mCrab, respectively. After data cleaning and dead-time correction, the total exposure time of the survey is ∼33 Ms.

⋆ Based on observations with INTEGRAL, an ESA project with the instruments and science data center funded by ESA member states (especially the PI countries: Denmark, France, Germany, Italy, Switzerland, Spain), Czech Republic, and Poland, and with the participation of Russia and the USA.

⋆⋆ Table 1 is only available in electronic form at the CDS via anonymous ftp to cdsarc.u-strasbg.fr (130.79.128.5) or via http://cdsweb.u-strasbg.fr/cgi-bin/qcat?J/A+A/475/775

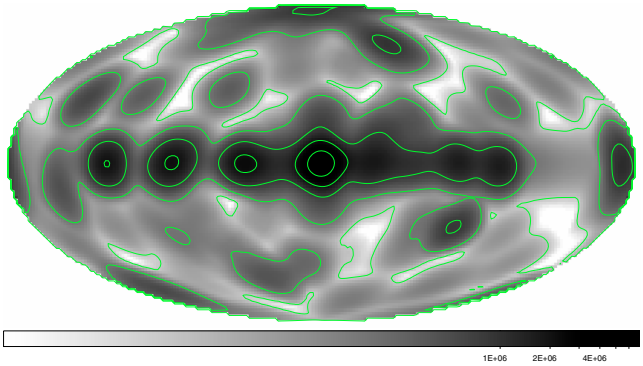

Fig. 1. Dead time-corrected exposure map of the survey. The green contours represent exposure levels of 10, 150, 800, 2000 and 4000 ks.

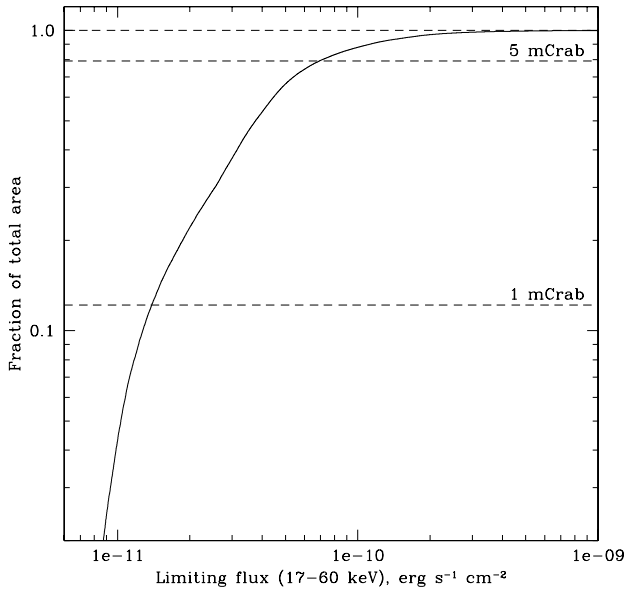

Fig. 2. Fraction of the sky surveyed as a function of the limiting flux for source detection with 5σ significance.

3. Data analysis

We analyzed the entire set of INTEGRAL observations at the level of individual pointings (science windows, SCWs), which have typical exposures of 2 ks. For each observation, the IBIS/ISGRI raw events list was converted to a sky image in our working energy band (17−60 keV). The employed algorithm of image reconstruction was previously described by Revnivtsev et al. (2004c) and Krivonos et al. (2005a). Here we outline only those steps that are essential for the present study.

We first accumulated raw detector images in the 17−60 keV energy band and cleaned them from bad and noisy pixels. The reconstruction starts with rebinning the raw detector images onto a grid with a pixel size equal to 1/3 of the mask pixel size. This is close but not exactly equal to the detector pixel size. Therefore, the rebinning causes a moderate loss in spatial resolution but enables a straightforward application of standard coded-mask reconstruction algorithms (e.g., Fenimore et al. 1981; Skinner et al. 1981). Essentially, for each sky location, the flux is calculated as the total flux in those detector pixels that "see" that location through the mask minus the flux in those detector pixels that are blocked by the mask.

The image reconstruction is based on the DLD deconvolution procedure (see the notations in Fenimore et al. 1981), with a mask pixel corresponding to $n \times n$ detector pixels (where $n = 3$). The original detector is treated as $n \times n$ independent detectors, and $n \times n$ independent sky images are reconstructed and then combined into a single image. A point source in such an image is represented by an $n \times n$ square. In our case, this leads to the effective point spread function (PSF) being approximately a square of 3×3 detector pixels, or $12' \times 12'$. After summing a large number of individual images, the 2D shape of the PSF can be approximated well by a Gaussian with $\sigma = 5'$.

The periodic structures in the IBIS mask give rise to parasitic peaks ("ghosts") in the images of real sources. Iterative removal of ghosts and determination of source flux are implemented as follows. First, a zero-order deprojection of the detector onto the sky is used to roughly estimate the fluxes of a predefined set of sources with known positions. Then the flux of the most statistically significant detected source is determined by fitting the normalization of the source's shadowgram, together with a background pattern (accumulated in "empty" fields). The estimated source contribution is then subtracted from the corresponding detector pixels. This procedure is repeated for all sources in the FOV of the telescope starting from the most significant one in descending order. The catalog of sources used for this procedure was renewed each time a new source was detected, and the image reconstruction was then redone for each observation containing the new source using the updated current catalog. The final catalog is presented in Table 1.

In general, due to the large number of pixels of the mask of IBIS and the ISGRI detector, the described procedure is quite stable. The addition of even a large (>50) number of artificial sources to the list of sources for the iterative removal procedure does not significantly affect the source flux determination.

Due to the periodic positions of the IBIS mask opaque pixels, the effective PSF of the instrument has substantial side peaks (so-called "ghosts"). If some source lies exactly at the position of a side peak caused by another source, the determination of its flux will interfere with the determination of the flux of the other source. We did encounter this problem with some sources in the Galactic center region. However, the presence of different telescope orientations in the INTEGRAL/IBIS dataset helps to significantly alleviate this problem.

The case of a bright source

Since the pattern of the shadowgram cast by a point source through the mask is not ideally known, the ghost removal procedure is not perfect. Some photon counts can be left or oversubtracted at specific several positions on the detector. This effect is usually small but can become significant for deep fields containing very bright sources. In this case, characteristic "crosses" and "rings" appear around the bright sources. The former artifact appears when the observational program of a bright source is dominated by starring pointings with a constant roll angle. A variable roll angle diminishes this effect but produces concentric structures. In practice, this means that, in regions with very bright sources, some source detections based on the criterion of exceeding a reasonable threshold, say 5σ, may be false. The level at which imperfect ghost removal starts to play a role depends on the observational pattern and typically corresponds to $\sim(3-5) \times 10^{-3}$ of the flux of the brightest source within the IBIS field of view. Therefore, the extracted list of excesses should always be checked "by eye" and cleaned out from these characteristic series of false detections around bright sources. It should be noted that such a cleaning introduces "dead zones" where a real source may be missed. We have verified that, in the worst case, the total

area of these zones does not exceed 100 deg^2, which constitutes a neglible fraction of the total area of our all-sky survey.

On applying the procedures described above, each observation is represented by a 28° × 28° sky image with a pixel size of 4′. The full analyzed data set contains 23 547 such images and comprises ∼35 Ms (dead time-corrected) worth of observations. We applied an additional filtering to the resulting images using information about the residual (after subtraction of point sources) rms signal-to-noise variations in the images. Those images having rms > 1.05 were excluded from the analysis. This resulted in an additional rejection of ∼7% of the pointings and finally left us with ∼33 Ms worth of clean observations.

An analysis of mosaic images built from observations covering the whole sky is complicated by various effects of projections onto a 2D plane. The most significant one is distortions of the PSF at positions far from the center of the projection. This leads to uncertainties in estimating the source position and flux. To avoid this effect, we followed an approach that had been developed for analyzing data distributed on a sphere. Specifically, we used a number of subroutines from the HEALPIX package (**H**ierarchical **E**qual **A**rea iso**L**atitude **Pix**elization of a sphere, Górski et al. 2005) to build a mosaiced sky. This technique provides an equal-area pixelization of the sphere and allows us to analyze all of the data uniformly. We produced a HEALPIX-based map of the whole sky with 12M pixels, which corresponds to a ∼3.4′ size for each sky pixel. The map was constructed by projecting individual IBIS/ISGRI images onto the HEALPIX all-sky frame.

3.1. Detection of sources

We searched for sources on three time scales: in individual SCWs (∼2 ks exposure time, typical sensitivity 20−30 mCrab), on images integrated over individual satellite orbits (∼200 ks, ∼4 mCrab), and on the time-averaged all-sky map (∼33 Ms).

The sources were detected using 20° × 20° projections of the HEALPIX all-sky image. Sources were searched as excesses on ISGRI sky maps, convolved with a Gaussian with $\sigma = 5'$, which resembles the effective PSF of IBIS/ISGRI very closely. Such a search is in fact a realization of the matched-filter technique, which maximizes the signal-to-noise ratio (S/N) for point sources.

The S/N distribution of pixels is dominated by the statistical noise and can be described by a Gaussian. In those sky regions that contain very bright point sources, the rms scatter of signal-to-noise ratios increases. However, this mainly occurs due to the presence of unsubtracted ghosts, which can be found by eye and removed.

There is a small mismatch between the sizes of the mask grid and the detector pixels, which leads to an imperfect redistribution of counts over the mask-aligned detector grid. However, this effect is minor, because the correlation length of the noise in the projected images is smaller than the size of the applied Gaussian filter. As a result, the originally measured variance of the distribution of pixel significances is slightly less than unity. To correct for this, we implemented a uniform rescaling of the error map for each sky projection. The correction factor was determined from each HEALPIX projection image and found to vary between 0.9 and 1.0. For sky fields containing a large number of point sources or for images of poor quality, this effect becomes less important than systematic biases introduced by the image reconstruction algorithm (Sect. 3). In such cases, the correction factor cannot be properly estimated, so we adapted it to be not greater than unity. In Fig. 3 we show the S/N distribution of the pixels of a 20° × 20° corrected sky map centered on some arbitrary position. This distribution (except for the positive bright tail produced by real sources) can be described by the normal distribution with unit variance and zero mean.

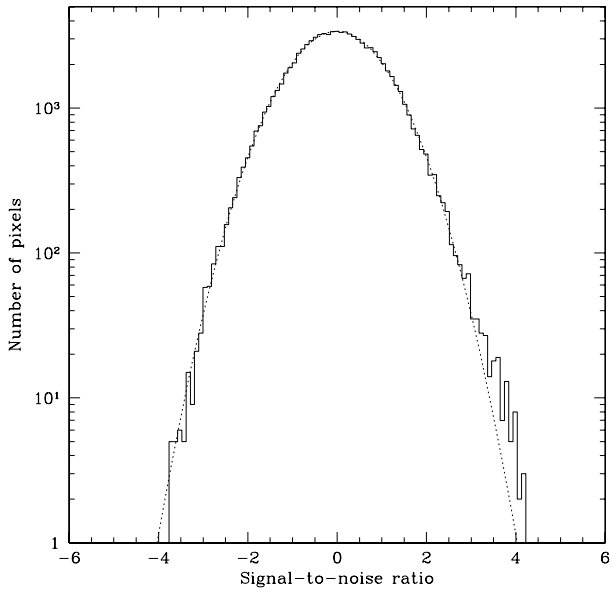

Fig. 3. Signal-to-noise ratio distribution (solid histogram) of the number of pixels in a 20° × 20° projection image of the sky around the position 15h28m00.0s, −28°00m00s (J2000). The dotted line represents the normal distribution with unit variance and zero mean.

We next specified a detection threshold in units of this clean "sigma" to search for sources in images. The lists of source candidates were then cleaned by eye from excesses forming characteristic patterns around bright sources. Taking the IBIS/ISGRI angular resolution into account, the all-sky map and maps accumulated during single revolutions contain ∼10^6 and 3×10^7 statistically independent pixels, respectively. We adopted the corresponding detection thresholds of $(S/N)_{\rm lim} > 5\sigma$ and $(S/N)_{\rm lim} > 5.5\sigma$ to ensure that the final catalog contains less than 1−2 spurious sources.

Apart from the main search described above, we detected several sources in special extended series of observations, such as the deep surveys of the Sagittarius and Crux spiral arm tangent regions (Molkov et al. 2004; Revnivtsev et al. 2006). Some of these sources fall below our detection threshold (5σ) on the all time-averaged map, which probably indicates their strong variability or transient nature.

We emphasize that for statistical studies only those sources should be used from the catalog that have time-averaged statistical significance higher than 5σ (see the flux column in Table 1 below).

3.2. Localization accuracy

We determined the positions of sources by fitting the centroid of a 2D Gaussian ($\sigma = 5'$) to the peak of the PSF-convolved source image. To estimate the accuracy of this method, we built the distribution of deviations of the measured positions of sources with known cataloged locations for a large number of INTEGRAL observations. The positional accuracy of sources detected by IBIS/ISGRI depends on the source significance (Gros et al. 2003; Bird et al. 2006). The estimated 68% confidence intervals for sources detected at 5−6, 10, and >20σ are 2.1′, 1.5′, and <0.8′, respectively.

4. Catalog

We detected a total of 403 sources in the 17−60 keV energy band over the whole sky. The full list of sources is presented in Table 1, and its content is described below.

Column (1) – source number in the catalog.
Column (2) – source name. For sources whose nature was known before their detection by INTEGRAL, their common names are given. Sources discovered by INTEGRAL or those whose nature was established thanks to INTEGRAL are named "IGR".
Columns (3,4) – source Equatorial (J2000) coordinates.
Column (5) – time-averaged source flux in mCrab units. A flux of 1 mCrab corresponds to 1.43×10^{-11} erg s^{-1} cm^{-2} for a source with a Crab-like spectrum.
Column (6) – general astrophysical type of the object: LMXB (HMXB) – low- (high-) mass X-ray binary, AGN – active galactic nucleus, SNR/PWN – supernova remnant, CV – cataclysmic variable, PSR – isolated pulsar or pulsar wind nebula, SGR – soft gamma repeater, RS CVn – coronally active binary star, SymbStar – symbiotic star, Cluster – cluster of galaxies.
Column (7) – additional notes and/or alternative source names.
Column (8) – references. These are mainly provided for new sources and are related to their discovery and/or nature.

We note that Bird et al. (2007) have recently performed a similar hard X-ray survey using INTEGRAL/IBIS/ISGRI data. The catalog of these authors contains 421 sources detected in five energy bands spanning 18−100 keV. Although a detailed comparison of this catalog with ours goes beyond the scope of the present paper, we may mention some important differences: (i) our dataset covers a number of extragalactic regions not covered by the survey of Bird et al. (2007); on the other hand, their dataset contains a considerable amount of data not available to us; (ii) Bird et al. (2007) used the standard INTEGRAL OSA software, whereas we used a software developed at the Space Research Institute (Moscow, Russia); (iii) the detection criterion adopted in our work allows not more than 1−2 spurious sources to be present in the whole catalog, while the catalog of Bird et al. (2007) may, as mentioned by authors, contain much more spurious sources.

4.1. Some peculiar sources

Galactic center source IGR J17456−2901

The sky density of hard X-ray sources is not very high – in general $N(>1$ mCrab$) < 0.1$ deg^{-2} – therefore the angular resolution of the IBIS telescope (∼12′) is usually enough to prevent source confusion. The only exceptional region is the Galactic center: in the close vicinity (within 1°) of Sgr A*, IBIS sees 10 sources.

At the position of Sgr A*, there is an additional hard X-ray excess, IGR J17456−2901. This source was originally reported by Revnivtsev et al. (2004c) and erroneously associated with the X-ray burster AX J17456−2901. Subsequent studies of this source are demonstrated that it is extended (Neronov et al. 2005; Bélanger et al. 2006) and is probably the superposition of a large number of faint point sources located in the Galactic nuclear stellar cluster (Krivonos et al. 2007). Note that, as is shown by Bélanger et al. (2006), the position of the centroid of the excess is displaced with respect to Sgr A*, at higher energies

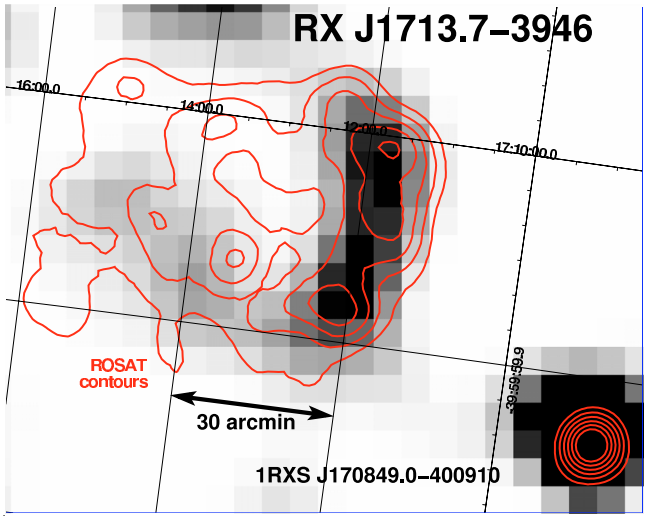

Fig. 4. INTEGRAL/IBIS hard X-ray (17−60 keV) image of the supernova remnant RX J1713.7−3946. The gray scale on the map is proportional to the hard X-ray flux. The map obtained by ROSAT in the soft X-ray (0.5−2.5 keV) band is shown by contours.

(∼70−100 keV), indicating that the nature of the high-energy source may be different from that of the 17−60 keV emission.

RX J1713.7−3946

Since IBIS is a coded-mask telescope, it is not well-suited to studying sources more extended than its angular resolution. However, if a source is only somewhat larger than the instrumental PSF, it is possible to obtain some limited information about the spatial structure of the source (see e.g. Renaud et al. 2006a,b).

In particular, there are four extended sources in our catalog that are not much larger than the IBIS PSF (∼12′): three clusters of galaxies (Oph, Perseus, and Coma) and the supernova remnant RX J1713.7−3946.

It is clearly seen (Fig. 4) that the supernova remnant RX J1713.7−3946 exhibits a clear extended structure (visible size in hard X-rays ∼24′). The significance of the hard X-ray detection varies along the extended structure between 4σ and 5σ (the statistical significance of the total extended emission is $>10\sigma$). The total exposure for this region is 5.3 Ms (dead-time corrected). To test the stability of the apparent spatial feature, we split the entire period of observations into four intervals and examined them individually. The extended structure is clearly present in each image and looks stable against the background of variable noise.

The supernova remnant RX J1713.7−3946 was discovered in soft X-rays during the ROSAT all-sky survey (Pfeffermann & Aschenbach 1996). An extended elliptical structure was found with a maximum extent of 70′ (see the red contours in Fig. 4). Not detecting of emission lines in the X-ray spectrum of RX J1713.7−3946 (ASCA, Koyama et al. 1997; Slane et al. 1999) was regarded as an indication that the observed X-rays is non-thermal emission from an expanding shell.

Recently, very high-energy (VHE) gamma-ray emission was discovered from the remnant by the H.E.S.S. experiment (Aharonian et al. 2006). The spatial correlation of the VHE emission intensity with the X-ray morphology confirms that cosmic-ray particles are being accelerated in the shell.

Here we report a detection of RX J1713.7−3946 in hard X-rays. The hard X-ray emission is probably synchrotron

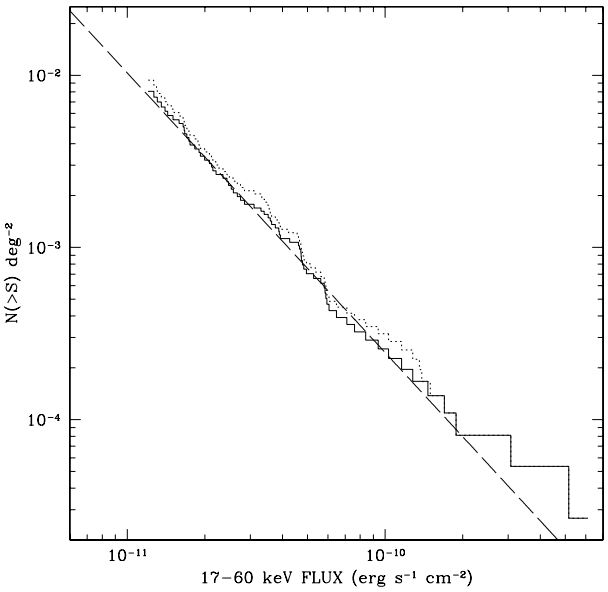

Fig. 5. Cumulative $\log N$–$\log S$ distribution of non-blazar AGNs in the energy band 17−60 keV obtained in the extragalactic sky ($|b| > 5°$, solid histogram). The best-fitting power law with a slope of 1.62 ± 0.15 and normalization of $(5.7 \pm 0.7) \times 10^{-3}$ deg^{-2} at a flux of 1 mCrab is shown by the dashed line. The dotted curve represents the $\log N$–$\log S$ distribution of all extragalactic sources including blazars and clusters of galaxies (except for unidentified sources).

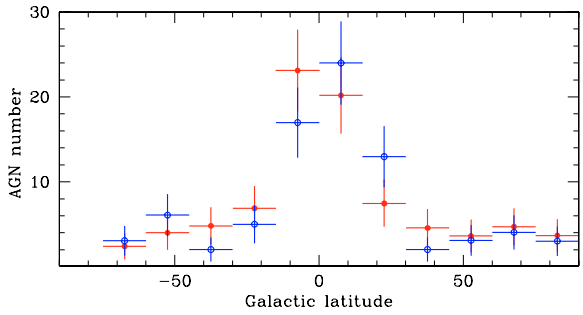

Fig. 6. Expected numbers of AGNs (filled red points) in 15°-wide Galactic-latitude strips (integrated over all Galactic longitudes) and the corresponding numbers of actually detected and identified AGNs (open blue points). The statistical uncertainties are shown by error bars.

emission of 100-TeV electrons accelerated in the shell (Koyama et al. 1995).

5. Extragalactic sources – AGNs

All sources in our catalog can be separated into two main classes, galactic and extragalactic (mainly AGNs). Under the assumption that AGNs are uniformly distributed over the sky (which is only a crude approximation of the real situation, see Sect. 6), we can construct the deepest number-flux function ever of hard X-ray emitting AGNs.

The catalog contains 130 objects[1] identified as AGNs (see also Sazonov et al. 2007[2]). Of these, 94 have a statistical significance higher than 5σ on the time-averaged map, including 85 emission-line AGNs (non-blazars) and 9 blazars. There are also 48 unidentified sources (34 found above the 5σ threshold on the averaged map and 14 transiently detected). The relative fraction of unidentified sources is much smaller for the extragalactic sky ($|b| > 5°$) than for the whole sky: the corresponding numbers of non-blazar AGNs and unidentified sources are 68 and 7 (excluding 6 transiently detected).

Since INTEGRAL observations cover the sky inhomogeneously, we should take the sensitivity map into account in constructing number-flux functions. In Fig. 5 we show the cumulative $\log N$–$\log S$ distribution of non-blazar AGNs derived at $|b| > 5°$ (excluding the 7 unidentified sources). It can be well fit by a power law: $N(>S) = AS^{-\alpha}$. Using a maximum-likelihood estimator (see e.g. Crawford et al. 1970), we determined the best-fit values of the slope and normalization: $\alpha = 1.62 \pm 0.15$ and $A = (5.7 \pm 0.7) \times 10^{-3}$ deg^{-2} at $S = 1$ mCrab. This implies that AGNs with fluxes exceeding our effective threshold $S_{\rm lim} = 0.8$ mCrab account for ∼1% of the intensity of the cosmic X-ray background in the 17−60 keV band, which was recently re-measured by INTEGRAL (Churazov et al. 2007).

We previously (Krivonos et al. 2005a) constructed a number-flux relation of extragalactic sources in a relatively small region of the sky (45° × 45°) around the Coma cluster of galaxies. The deep (∼500 ks) observations of the Coma were used to study a sample of 12 excesses in that field. After correcting for the expected number of false detections and fitting the resulting $\log N$–$\log S$ relation by a power law with the Euclidean-geometry slope of 3/2, the surface density of hard X-ray sources above a 20−50 keV flux threshold of 10^{-11} erg s^{-1} cm^{-2} (∼1 mCrab) was found to be $(1.4 \pm 0.5) \times 10^{-2}$ deg^{-2}. This value is higher than the average surface number density of AGNs in the $|b| > 5°$ sky determined above, which probably reflects the large-scale overdensity of galaxies in the general direction of the Coma cluster (see Sect. 6).

Using the derived $\log N$–$\log S$ distribution, we can compare the numbers of AGNs detected during the survey in different parts of the sky with the numbers expected under the assumption of uniform spatial distribution of sources. We find good agreement between these numbers within the statistical errors for 15° × 360° strips cut parallel to the Galactic plane (Fig. 6). Even in the Galactic plane region ($|b| < 5°$), which was excluded from our calculation of the number-flux function, the expected number of AGNs exceeding the detection threshold (18.4) is compatible with the number of detected and identified AGNs (16). This suggests that most of the unidentified sources in the Galactic plane region are of Galactic, rather than extragalactic, origin. This tentative conclusion of course rests on our assumption that AGNs are distributed uniformly on very large scales over the sky, which is in fact approximately true only for relatively distant objects ($D \gtrsim 70$ Mpc, see the next section) and much less so for more nearby AGNs, which constitute approximately half of our sample.

If we now include all the identified AGNs detected in the Galactic plane region into the calculation of the AGN number-flux function (thus increasing the total number of non-blazar AGNs to 85 and extending the calculation to the whole sky), we find $\alpha = 1.50 \pm 0.13$ and $A = (5.4 \pm 0.6) \times 10^{-3}$ deg^{-2} at 1 mCrab, i.e. virtually the same values as for the $|b| > 5°$ sky.

[1] Four additional sources: IGR J02466−4222, IGR J02524−0829, IGR J18578−3405, and IGR J18249−3243, have a suspected AGN origin.

[2] After publication of the INTEGRAL AGN catalog by Sazonov et al. (2007), three sources have been added to the AGN list: ESO 005-G004, IGR J14561−3738, and SWIFT 0920.8−0805.

6. Signatures of a large-scale structure in the population of hard X-ray AGNs

It is now widely accepted that practically every galaxy in the local Universe has a supermassive black hole and that some of these black holes are AGNs with widely ranging luminosities (see e.g., Richstone et al. 1998; Kormendy 2001, for a review). Therefore, it is reasonable to assume that the space density of X-ray emitting AGNs is proportional to that of normal galaxies.

The spatial distribution of galaxies in the local Universe is inhomogeneous. The gravitational attraction of matter in the Universe has formed different structures with sizes[3] up to ~100 Mpc. On larger scales, matter is distributed more or less uniformly, whereas there is strong inhomogeneity on smaller scales. The contrast in matter density between galaxy concentrations and voids can reach an order of magnitude and more (see e.g. Rees 1980; Davis & Peebles 1983; Bahcall & Burgett 1986). As our sample of hard X-ray emitting AGNs mostly probes the nearby Universe out to distances ~200 Mpc, we have the possibility of seeing similarly strong inhomogeneities in the distribution of nearby AGNs.

To this end, we estimated the space densities of AGNs in different directions of the sky. Due to the relatively small size of our sample, we assumed that the AGN number density is constant along a given line of sight, while the shape of the AGN luminosity function is invariant in the local Universe. We adopted this shape from Sazonov et al. (2007), who calculated the hard X-ray luminosity function for the high Galactic latitude ($|b| > 5°$) sky using practically the same sample of AGNs as in the present study.

Under these assumptions and using the sensitivity map of the survey, we determined the normalization of the luminosity function within spherical cones drawn around multiple directions in the sky through comparison of the expected and measured numbers of AGNs in these cones. We adopted the half-opening angle of the cones to be $\theta = 45°$ in order to achieve reasonably good angular resolution of the resulting map and still have a significant number of AGNs in each cone. To optimize our sensitivity to anisotropies in the spatial distribution of AGNs, we restricted ourselves to distances <70 Mpc, at which maximal contrasts in galaxy numbers are expected (see e.g. Rowan-Robinson et al. 2000).

In Sect. 3 we have demonstrated that most of the extragalactic objects detectable by INTEGRAL in the Galactic plane region are probably already identified, hence we can use the all-sky sample of AGNs for our analysis.

The resulting map of the number density of nearby AGNs over the sky is shown in Fig. 7. The density is given in units of 2×10^{-4} Mpc^{-3} at luminosities higher than 10^{42} erg s^{-1} (17−60 keV), which is approximately the average local density of AGNs (Sazonov et al. 2007). Prominent large-scale concentrations of AGNs can be seen in the northern (to the right) and southern (to the left) Galactic hemispheres.

We can assess the statistical significance of these anisotropies by considering the probability of by chance having the observed contrast, i.e. the difference between the maximum and minimum numbers of sources within the search cone over the sky.

To this end, we made use of the AGN luminosity function from Sazonov et al. (2007) and the IBIS/ISGRI exposure map to construct an all-sky map of the expected surface number density of nearby (<70 Mpc) AGNs detectable during the survey,

[3] Hereafter we adopt $H_0 = 73$ km s^{-1} Mpc^{-1}.

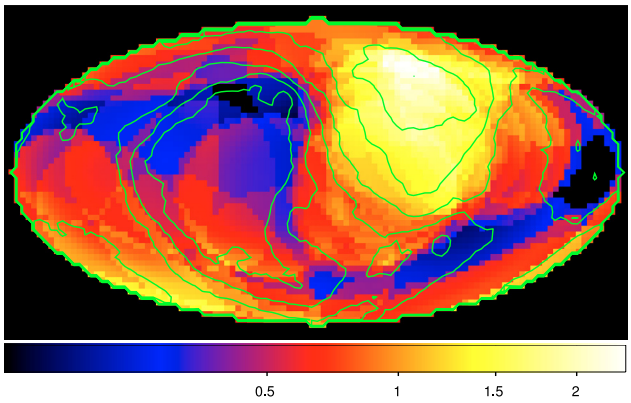

Fig. 7. 2D-map of the AGN number density in the local Universe. This map was constructed in Galactic coordinates using the sample of 39 AGNs located at distances $D < 70$ Mpc. Shown for each pixel is the estimated normalization of the AGN luminosity function within a spherical cone with a half-opening angle of 45° around that direction. The density is given in units of 2×10^{-4} Mpc^{-3} at luminosities higher than 10^{42} erg s^{-1} (17−60 keV), which is the average local density of AGNs (Sazonov et al. 2007). Green contours show the surface number density of galaxies detected during the IRAS PSCz survey at distances $D < 70$ Mpc.

assuming that the spatial distribution of AGNs in the local Universe is homogeneous. According to this map, a total of 43.8 AGNs with luminosities higher than 10^{41} erg s^{-1} are expected to be detected from the considered volume of space, while the actual number of observed AGNs is 39. This small difference can be attributed to the AGN sample that was used by Sazonov et al. (2007) to derive the luminosity function being slightly different from the current one, in particular in the absence of AGNs located at low Galactic latitudes ($|b| < 5°$); there would be no difference if both samples were identical.

Based on this map of expected AGN surface number density, we then simulated (assuming Poisson statistics) a large number of AGN samples, selected those of them with the total number of sources being equal to the observed number (39), and constructed the corresponding 2D-maps of the AGN number density using the same search cone as for the observed map (Fig. 7). We then looked for those maps where the difference between the maximum and minimum numbers of sources within the search cone was larger than the observed one (maximum − minimum = 22 − 0 = 22). In this way we found that the probability that the observed map is a random realization of a homogeneous distribution of AGNs in the local Universe is 2.3×10^{-4}.

If we take into account that the high and low AGN number density regions appear to correlate with known (from surveys of both infrared galaxies, e.g. Rowan-Robinson et al. 2000, and X-ray clusters of galaxies, e.g. Kocevski & Ebeling 2006) over- and under-dense regions in the local Universe, respectively, the statistical significance of the found spatial inhomogeneity will be much higher.

The discovered anisotropy of AGNs agrees well with the known distribution of matter in the local Universe. The large-scale feature in the northern Galactic hemisphere is consistent with the position of the highest mass concentrations in the local Universe: the nearby Virgo cluster (~18 Mpc, $\sim 1.2 \times 10^{15}$ $M_\odot$ Fouqué et al. 2001; Tonry et al. 2000) and the more distant and massive Great Attractor (~65 Mpc, $(1-5) \times 10^{16}$ $M_\odot$, Lynden-Bell et al. 1988; Tonry et al. 2000). The southern structure is consistent with the Perseus-Pisces supercluster (~50 Mpc, $(7-9) \times 10^{15}$ $M_\odot$, Hanski et al. 2001).

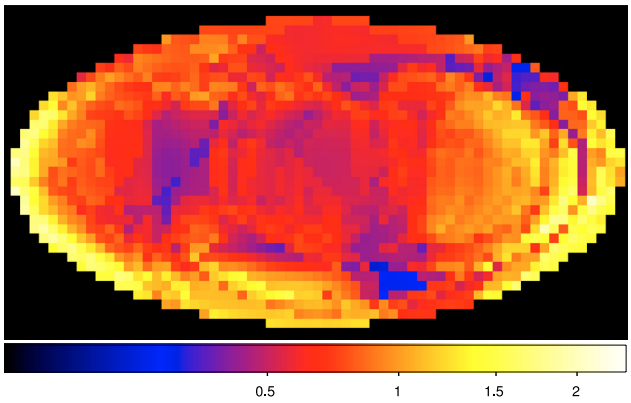

Fig. 8. 2D-map of the number density of AGNs at distances $D >$ 70 Mpc. See Fig. 7 for the description. This map is based on 40 objects.

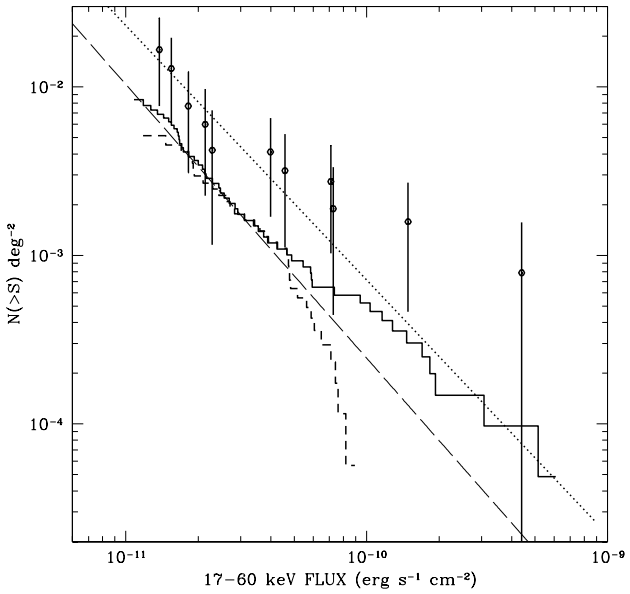

Fig. 9. Number-flux functions of extragalactic sources (excluding blazars and clusters of galaxies) measured in different sky regions. The $\log N$–$\log S$ relations for sources in two hemispheres, in the direction of the IRAS dipole $l = 268°$, $b = 27°$ (Lahav et al. 1988) and in the opposite direction, are shown by the solid and dashed histograms, respectively. The long–dashed line represents the best-fitting $\log N$–$\log S$ distribution for the entire sky excluding the Galactic plane ($|b| > 5°$, see Fig. 5). The open circles with error bars represent the number-flux relation of extragalactic sources obtained in the $45° \times 45°$ region around the Coma cluster (Krivonos et al. 2005a) in the 20−50 keV energy band. The flux was converted to the 17−60 keV energy band assuming Crab spectrum. The dotted line shows the corresponding $N \propto S^{-3/2}$ fit.

To demonstrate the similarity between the distributions of hard X-ray emitting AGNs and matter over the sky better, we used the IRAS PSC redshift survey (Saunders et al. 2000). We selected galaxies located at distances <70 Mpc and having a far-infrared flux of $S_{60\,\mu m} > 1$ Jy. The IRAS PSCz survey covers approximately 83% of the sky due to the presence of the so-called zone of avoidance, a sky region to the north and to the south from the Galactic equator where Galaxy obscures the IR emission. To fill this gap during the construction of the map of densities of IR galaxies, we assumed that the number density of galaxies hidden behind the Galactic plane (10 degrees to the north and to the south of the equator) is constant and equals the all-sky average value. Contours of the number density map of IRAS galaxies are shown in Fig. 7. We emphasize that this comparison is fairly approximate and only reflects the distribution of the projected mass. A detailed study of the correlation between the spatial distributions of hard X-ray emitting AGNs and matter in the local Universe will be presented elsewhere.

It is obvious from the above discussion that any estimate of the AGN surface number density based on a small area of the sky may be biased. This was apparently the case for our survey in the $\sim 45° \times 45°$ region around the Coma cluster (Krivonos et al. 2005a), where a high surface number density of relatively nearby ($D \lesssim 70$ Mpc) AGNs was found (see Sect. 5). Indeed, the observed region is located in the vicinity of the prominent large-scale structure in the northern Galactic hemisphere (see Fig. 7), which can affect the estimation of AGN surface number density. As can be seen from Fig. 9, the obtained extragalactic $\log N$–$\log S$ distribution in the Coma region is higher than (but statistically consistent with) the all-sky determination. To better demonstrate the strong contrast in the distribution of AGNs over the sky, we calculated the sensitivity-corrected $\log N$–$\log S$ distributions of AGNs in the two hemispheres defined by the direction of motion of the Local Group: $l = 268°, b = 27°$, as measured by IRAS (Lahav et al. 1988). These distributions are shown in Fig. 9. The number of bright sources ($S \gtrsim 10^{-10}$ erg s^{-1} cm^{-2}), for which our survey is almost 100% complete in both hemispheres, exhibits a contrast as high as 11:1. For a uniform spatial distribution of AGN, the probability of observing such a contrast by chance is only 9.7×10^{-4}.

We explicitly calculated the AGN luminosity functions in both hemispheres defined above and found their shapes to be consistent with that of the all-sky average luminosity function determined by Sazonov et al. (2007). This supports the hypothesis that the found anisotropy mostly reflects the inhomogeneous distribution of matter in the local Universe rather than generic variations in the AGN luminosity function.

Figure 9 demonstrates that most of the observed anisotropy in the distribution of AGNs over the sky is due to the closest (brightest) AGNs. Inclusion of sources located at progressively larger distances is expected to decrease the surface number density variations over the sky (Rowan-Robinson et al. 2000). To demonstrate this, we built a map of the number density of AGNs located at $D > 70$ Mpc (Fig. 8), which should be compared with the one for nearby AGNs ($D < 70$ Mpc, Fig. 7). It can be seen that, the more distant AGNs are distributed more uniformly across the sky, their distribution does not demonstrate statistically significant anisotropy: the corresponding probability of finding the observed contrast in the number of AGN by chance within the search cone is 92%.

Figure 9 shows the $\log N$–$\log S$ distribution previously obtained in the Coma region. This number-flux relation lies higher than the all-sky average due to the overdensity of galaxies in this relatively small region of the sky (1243 sq. deg), including two bright AGNs, NGC 4151, and NGC 4388. As a result, the resolved fraction of the CXB in this region is also high, ~3%. As already mentioned above, the resolved fraction of the CXB for the whole sky is only ~1%. This last value is consistent with what is reported by Beckmann et al. (2006) based on their analysis of INTEGRAL observations covering 25 000 sq. deg of the sky.

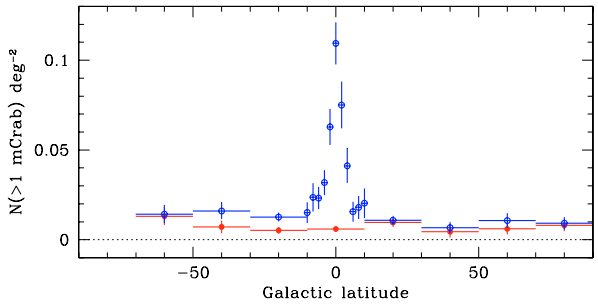

Fig. 10. Surface number density of (>5σ) sources with flux >1 mCrab as a function of Galactic latitude. Open blue and filled red points represent all and (identified) extragalactic sources, respectively. The dashed line represents the normalization of the all-sky extragalactic log N–log S function.

7. Galactic sources

The presence of a large number of Galactic sources in the INTEGRAL all-sky catalog is obvious from the large overdensity of sources near the Galactic plane. As a demonstration we built sensitivity-corrected cumulative number-flux functions for all (>5σ) sources in 15° Galactic-latitude bins. The derived surface number density of sources as a function of Galactic latitude is shown in Fig. 10.

The vast majority of sources in the Galactic plane are low- and high-mass X-ray binaries (>70% in total, excluding unidentified sources). The number-flux function of all sources at $|b| < 5°$ (Fig. 11), is much flatter than that of extragalactic sources at $|b| > 5°$ (Forman et al. 1978) and reflects the luminosity functions of the dominant Galactic source populations (see e.g. Grimm et al. 2002). A detailed study of Galactic sources based on the INTEGRAL all-sky survey will be presented elsewhere.

8. Conclusion

We have presented the all-sky hard X-ray (17−60 keV) survey performed by the IBIS coded-mask telescope of the INTEGRAL observatory. The total dead-time corrected exposure of the survey is 33 Ms. Approximately 12% and 80% of the whole sky have been covered down to limiting fluxes of 1 and 5 mCrab, respectively. The survey allowed us for the first time to study the population of hard X-ray sources in an unbiased manner, without strong influence of a combination of limited sky coverage and observing program targeting brightest objects on the sky.

Our catalog contains 403 detected sources. Of these, 217 are of Galactic origin (90 LMXBs, 76 HMXBs, 21 CVs, 6 active stars, and other types) and 137 are extragalactic, including 130 AGNs, 4 AGN candidates, and 3 clusters of galaxies. There remain 48 unidentified sources including excesses above the 5σ level on the time-averaged map (34) and transient detections (14). Only 13 unidentified excesses are located in the extragalactic sky ($|b| > 5°$) and have significance >5σ: 7 on the average map and 6 transients. The catalog includes 138 sources discovered by INTEGRAL, 15 of which are reported here for the first time.

A number of sources detected by INTEGRAL/IBIS have counterparts in the TeV energy band. In this paper we have presented the map of extended hard X-ray (17−60 keV) emission of the supernova remnant RX J1713.7−3946 for the first time.

We explored the spatial distribution of AGNs in the local Universe. The cumulative log N–log S function of AGNs derived away from the Galactic plane (at $|b| > 5°$) can be fit well by a power law $N(>S) = (5.7 \pm 0.7) \times 10^{-3} S^{-1.62 \pm 0.15}$ deg^{-2} (fluxes in mCrab units). This implies that ∼1% of the CXB at 17−60 keV is directly resolved by INTEGRAL.

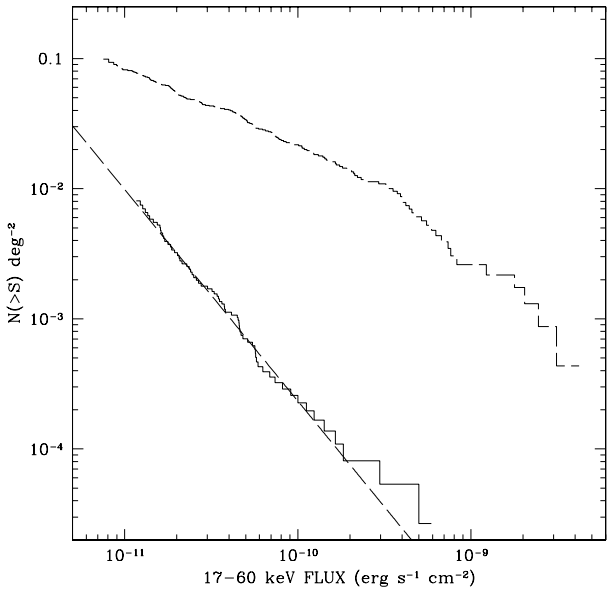

Fig. 11. Cumulative log N–log S distribution in the energy band 17−60 keV of all sources in the Galactic plane region ($|b| < 5°$, dashed histogram) in comparison with that of AGNs at high latitudes ($|b| > 5°$, solid histogram). The dashed line represents the best-fitting power law to the number-flux relation of AGNs.

We demonstrated that local (≲70 Mpc) AGNs are inhomogeneously distributed in space, largely following the large-scale structure. In particular, significant concentrations of AGNs were found in the regions of the sky around the Virgo cluster, the Great Attractor, and the Perseus-Picses supercluster.

Acknowledgements. The INTEGRAL data used here were obtained from the European and Russian INTEGRAL Science Data Centers. We thank S. Molkov and S. Grebenev for scrupulously checking the catalog and the anonymous referee for valuable comments. The work was supported by the DFG Schwerpunkt program 1177 "Witnesses of Cosmic History: Formation and evolution of galaxies, black holes, and their environment", by the President of the Russian Federation (through the program of support at leading scientific schools, project NSH-1100.2006.2), by the Presidium of the Russian Academy of Sciences/RAS (the program "Origin and evolution of stars and galaxies"), by the Division of Physical Sciences of the RAS (the program "Extended objects in the Universe"), and by the Russian Basic Research Foundation (projects 05-02-16540 and 07-02-01051). AL acknowledges the support from the Russian Science Support Foundation.

9. References for the catalog

(1) Donato et al. (2005), (2) Sazonov et al. (2005), (3) Masetti et al. (2004), (4) Masetti et al. (2006c), (5) Brandt et al. (2005), (6) Sunyaev et al. (2003a), (7) Masetti et al. (2006e), (8) Masetti et al. (2006b), (9) Bassani et al. (2006), (10) Sguera et al. (2006), (11) Lutovinov et al. (2004a), (12) Lubinski et al. (2005), (13) den Hartog et al. (2004a), (14) Grebenev et al. (2004b), (15) Smith et al. (2006), (16) Kretschmar et al. (2004), (17) Chernyakova et al. (2005a), (18) in't Zand & Heise (2004), (19) Rodriguez et al. (2004), (20) Morelli et al. (2006), (21) Revnivtsev et al. (2004b), (22) Kuulkers et al. (2006), (23) Revnivtsev et al. (2006), (24) Lutovinov & Revnivtsev (2003), (25) Lutovinov et al. (2005a), (26) Bykov et al. (2004), (27) Bassani et al. (2005), (29) Pavlinskii et al. (1992), (30) Lutovinov et al. (2003c), (31) in't Zand (2005), (32) Bikmaev et al. (2006a), (33) Negueruela & Smith (2006), (34) Produit et al. (2004), (35) Barlow et al. (2005), (36) Barlow et al. (2006), (37) Walter et al. (2006),

(38) Molkov et al. (2004), (39) Bykov et al. (2006), (40) Liu et al. (2000), (41) Liu et al. (2001), (42) Rodriguez et al. (2005), (43) den Hartog et al. (2005), (44) Bird et al. (2006), (45) den Hartog et al. (2004b), (46) Ubertini et al. (2005), (47) Malizia et al. (2005), (48) Aleksandrovich et al. (1995), (49) Cornelisse et al. (2006), (50) Bikmaev et al. (2006b), (51) Chernyakova et al. (2005b), (52) Reig et al. (2005), (53) Hannikainen et al. (2003), (54) Sunyaev et al. (2003b), (55) Burenin et al. (2006b), (56) Negueruela et al. (2005), (57) Keek et al. (2006), (58) Krivonos et al. (2005b), (59) Grebenev et al. (2004a), (60) Burenin et al. (2006a), (61) Grebenev et al. (2005b), (62) Kuiper et al. (2006), (63) Masetti et al. (2006a), (64) Lutovinov et al. (2004b), (65) Tueller et al. (2005), (66) Halpern (2006), (67) Masetti et al. (2006d), (68) Masetti et al. (2005), (69) Karasev et al. (2007), (70) Brandt et al. (2006), (71) Chernyakova et al. (2003), (72) Gänsicke et al. (2005), (73) Turler et al. (2005), (74) Grebenev et al. (2005a), (75) Gotz et al. (2006), (76) Krivonos et al. (2007), (77) Sazonov et al. (2007), (78) Rea et al. (2006), (79) Bélanger et al. (2006), (80) Palmer et al. (2005), (81) Torres et al. (2005), (82) Sguera et al. (2007), (83) Tomsick et al. (2006), (84) Revnivtsev et al. (2003a), (85) Courvoisier et al. (2003), (86) Walter et al. (2004), (87) Tomsick et al. (2003), (88) Revnivtsev et al. (2003b), (89) Patel et al. (2004), (90) Bodaghee et al. (2006), (91) Tomsick et al. (2004), (92) Molkov et al. (2003), (93) Lutovinov et al. (2005b), (94) Kuulkers et al. (2003), (95) Revnivtsev et al. (2003c), (96) Lutovinov et al. (2003a), (97) Lutovinov et al. (2005c), (98) Revnivtsev et al. (2004c), (99) Augello et al. (2003), (100) Lutovinov et al. (2003b) (101) Sazonov et al., in preparation, (102) Masetti et al. (2007a), (103) Grebenev et al. (2005c), (104) Grebenev & Sunyaev (2004), (105) Beckmann et al. (2005), (106) Grebenev et al. (2005d), (107) Kuiper et al. (2005), (108) Masetti et al. (2007b).

References

Aharonian, F., Akhperjanian, A. G., Bazer-Bachi, A. R., et al. 2006, A&A, 449, 223
Aleksandrovich, N. L., Aref'ev, V. A., Borozdin, K. N., Syunyaev, R. A., & Skinner, G. K. 1995, Astron. Lett., 21, 431
Augello, G., Iaria, R., Robba, N., et al. 2003, ApJ, 596, L63
Bahcall, N. A., & Burgett, W. S. 1986, ApJ, 300, L35
Barlow, E. J., Bird, A., Clark, D., et al. 2005, A&A, 437, L27
Barlow, E. J., Knigge, C., Bird, A. J., et al. 2006, MNRAS, 372, 224
Bassani, L., De Rosa, A., Bazzano, A., et al. 2005, ApJ, 634, L21
Bassani, L., Molina, M., Malizia, A., et al. 2006, ApJ, 636, L65
Bazzano, A., Stephen, J. B., Fiocchi, M., et al. 2006, ApJ, 649, L9
Beckmann, V., Kennea, J. A., Markwardt, C., et al. 2005, ApJ, 631, 506
Beckmann, V., Soldi, S., Shrader, C. R., Gehrels, N., & Produit, N. 2006, ApJ, 652, 126
Bélanger, G., Goldwurm, A., Renaud, M., et al. 2006, ApJ, 636, 275
Bikmaev, I. F., Sunyaev, R. A., Revnivtsev, M. G., & Burenin, R. A. 2006a, Astron. Lett., 32, 221
Bikmaev, I. F., Sunyaev, R. A., Revnivtsev, M. G., & Burenin, R. A. 2006b, Astron. Lett., 32, 588
Bird, A. J., Barlow, E. J., Bassani, L., et al. 2006, ApJ, 636, 765
Bird, A. J., Malizia, A., Bazzano, A., et al. 2007, ApJS, 170, 175
Bodaghee, A., Walter, R., Zurita Heras, J., et al. 2006, A&A, 447, 1027
Brandt, S., Kuulkers, E., Bazzano, A., et al. 2005, Astron. Telegram, 622, 1
Brandt, S., Budtz-Jørgensen, C., & Chenevez, J. 2006, Astron. Telegram, 778, 1
Burenin, R., Mescheryakov, A., Revnivtsev, M., Bikmaev, I., & Sunyaev, R. 2006a, The Astronomer's Telegram, 880, 1
Burenin, R., Mescheryakov, A., Sazonov, S., et al. 2006b, Astron. Telegram, 883, 1
Bykov, A., Krassilshchikov, A., Uvarov, Yu., et al. 2004, A&A, 427, L21
Bykov, A., Krassilshchikov, A., Uvarov, Yu., et al. 2006, ApJ, 649, L21
Chelovekov, I., Grebenev, S., & Sunyaev, R. 2006, Astron. Lett., 32, 456
Chelovekov, I., Grebenev, S., & Sunyaev, R. 2007, in Proceedings of the 6th INTEGRAL Workshop, The Obscured Universe (3−7 July 2006, Moscow), ESA SP-622, 2007, accepted
Chernyakova, M., Lutovinov, A., Capitanio, F., Lund, N., & Gehrels, N. 2003, Astron. Telegram, 157, 1
Chernyakova, M., Courvoisier, T., Rodriguez, J., & Lutovinov, A. 2005a, Astron. Telegram, 519, 1
Chernyakova, M., Lutovinov, A., Rodríguez, J., & Revnivtsev, M. 2005b, MNRAS, 364, 455
Cornelisse, R., Charles, P. A., & Robertson, C. 2006, MNRAS, 366, 918
Courvoisier, T., Walter, R., Rodriguez, J., Bouchet, L., & Lutovinov, A. 2003, IAUC, 8063, 1
Crawford, D. F., Jauncey, D. L., & Murdoch, H. S. 1970, ApJ, 162, 405
Donato, D., Sambruna, R. M., & Gliozzi, M. 2005, A&A, 433, 1163
Davis, M., & Peebles, P. J. E. 1983, ARA&A, 21, 109
den Hartog, P., Hermsen, W., Kuiper, L., et al. 2004a, Astron. Telegram, 261, 1
den Hartog, P., Kuiper, L., Corbet, R., et al. 2004b, Astron. Telegram, 281, 1
den Hartog, P., Kuiper, L., Hermsen, W., et al. 2005, Astron. Telegram, 394, 1
Hopkins, P. F., Hernquist, L., Cox, T. J., et al. 2006, ApJS, 163, 1
Fenimore, E. E., & Cannon, T. M. 1981, Applied Optics, 20, 1858
Forman, W., Jones, C., Cominsky, L., et al. 1978, ApJS, 38, 357
Fouqué, P., Solanes, J. M., Sanchis, T., & Balkowski, C. 2001, A&A, 375, 770
Gänsicke, B. T., Marsh, T. R., Edge, A., et al. 2005, MNRAS, 361, 141
Górski, K. M., Hivon, E., Banday, A. J., et al. 2005, ApJ, 622, 759
Gotz, D., Schanne, S., Rodriguez, J., et al. 2006, Astron. Telegram, 813, 1
Grebenev, S. A., & Sunyaev, R. A. 2004, The Astronomer's Telegram, 342, 1
Grebenev, S. A., Ubertini, P., Chenevez, J., Orr, A., & Sunyaev, R. A. 2004a, Astron. Telegram, 275, 1
Grebenev, S., Ubertini, P., Chenevez, J., et al. 2004b, Astron. Telegram, 350, 1
Grebenev, S. A., Molkov, S. V., & Sunyaev, R. A. 2005a, Astron. Telegram, 467, 1
Grebenev, S. A., Molkov, S. V., & Sunyaev, R. A. 2005b, The Astronomer's Telegram, 616, 1
Grebenev, S. A., Molkov, S. V., & Sunyaev, R. A. 2005c, The Astronomer's Telegram, 444, 1
Grebenev, S. A., Bird, A. J., Molkov, S. V., et al. 2005d, The Astronomer's Telegram, 457, 1
Grimm, H.-J., Gilfanov, M., & Sunyaev, R. 2002, A&A, 391, 923
Gros, A., Goldwurm, A., Cadolle-Bel, M., et al. 2003, A&A, 411, L179
Halpern, J. P. 2006, Astron. Telegram, 847, 1
Hannikainen, D., Rodriguez, J., Pottschmidt, K., et al. 2003, IAUC, 8088, 1
Hanski, M. O., Theureau, G., Ekholm, T., & Teerikorpi, P. 2001, A&A, 378, 345
in't Zand, J. J. M. 2005, A&A, 441, L1
in't Zand, J. J. M., & Heise, J. 2004, Astron. Telegram, 362, 1
Karasev, D. I., Lutovinov, A. A., & Grebenev, S. A. 2007, Astron. Lett., 33, 159
Keek, S., Kuiper, L., & Hermsen, W. 2006, The Astronomer's Telegram, 810, 1
Kocevski, D. D., & Ebeling, H. 2006, ApJ, 645, 1043
Kormendy, J. 2001, Rev. Mex. Astron. Astrofis. Conf. Ser., 10, 69
Kormendy, J., & Richstone, D. 1995, ARA&A, 33, 581
Koyama, K., Petre, R., Gotthelf, E. V., et al. 1995, Nature, 378, 255
Koyama, K., Kinugasa, K., Matsuzaki, K., et al. 1997, PASJ, 49, L7
Kretschmar, P., Mereghetti, S., Hermsen, W., et al. 2004, Astron. Telegram, 345, 1
Krivonos, R., Vikhlinin, A., Churazov, E., et al. 2005a, ApJ, 625, 89
Krivonos, R., Molkov, S., Revnivtsev, M., et al. 2005b, Astron. Telegram, 545, 1
Krivonos, R., Revnivtsev, M., Churazov, E., et al. 2007, A&A, 463, 957
Kuiper, L., Jonker, P., Hermsen, W., & O'Brien, K. 2005, Astron. Telegram, 654, 1
Kuiper, L., Keek, S., Hermsen, W., Jonker, P. G., & Steeghs, D. 2006, Astron. Telegram, 684, 1
Kuulkers, E., Lutovinov, A., Parmar, A., et al. 2003, Astron. Telegram, 149, 1
Kuulkers, E., Shaw, S., Paizis, A., et al. 2006, Astron. Telegram, 874, 1
Lahav, O., Lynden-Bell, D., & Rowan-Robinson, M. 1988, MNRAS, 234, 677
Lahav, O., Fabian, A. C., Edge, A. C., & Putney, A. 1989, MNRAS, 238, 881
Landi, R., Tueller, J., Markwardt, C., Hill, A., & Fiocchi, M. T. 2007, The Astronomer's Telegram, 992, 1
Levine, A. M., Lang, F. L., Lewin, W. H. G., et al. 1984, ApJS, 54, 581
Liu, Q. Z., van Paradijs, J., & van den Heuvel, E. P. J. 2000, A&AS, 147, 25
Liu, Q. Z., van Paradijs, J., & van den Heuvel, E. P. J. 2001, A&A, 368, 1021
Lubinski, P., Gadolle Bel, M., von Kienlin, A., et al. 2005, Astron. Telegram, 469, 1
Lutovinov, A. A., & Revnivtsev, M. G. 2003, Astron. Lett., 29, 719
Lutovinov, A., Walter, R., Belanger, R., et al. 2003a, Astron. Telegram, 155, 1
Lutovinov, A., Shaw, S., Foschini, L., & Paul, J. 2003b, Astron. Telegram, 154, 1
Lutovinov, A., Rodriguez, J., Produit, N., & Paul, J. 2003c, Astron. Telegram, 151, 1
Lutovinov, A., Rodriguez, J., Budtz-Jorgensen, C., et al. 2004a, Astron. Telegram, 329, 1
Lutovinov, A., Bel, M. C., Belanger, G., et al. 2004b, Astron. Telegram, 328, 1
Lutovinov, A., Rodriguez, J., Revnivtsev, M., & Shtykovskiy, P. 2005a, A&A, 433, L41
Lutovinov, A., Revnivtsev, M., Gilfanov, M., et al. 2005b, A&A, 444, 821

Lutovinov, A., Revnivtsev, M., Molkov, S., & Sunyaev, R. 2005c, A&A, 430, 997
Lynden-Bell, D., Faber, S. M., Burstein, D., et al. 1988, ApJ, 326, 19
Malizia, A., Bassani, L., Stephen, J., et al. 2005, ApJ, 630, L157
Masetti, N., Palazzi, E., Bassani, L., Malizia, A., & Stephen, J. B. 2004, A&A, 426, L41
Masetti, N., Bassani, L., Bird, A., & Bassano, A. 2005, Astron. Telegram, 528,1
Masetti, N., Morelli, L., Palazzi, E., et al. 2006a, Astron. Telegram, 783, 1
Masetti, N., Morelli, L., Palazzi, E., et al. 2006b, A&A, 459, 21
Masetti, N., Pretorius, M. L., Palazzi, E., et al. 2006c, A&A, 449, 1139
Masetti, N., Bassani, L., Dean, A. J., Ubertini, P., & Walter, R. 2006d, The Astronomer's Telegram, 715, 1
Masetti, N., Bassani, L., Bazzano, A., et al. 2006e, A&A, 455, 11
Masetti, N., Cellone, S. A., Landi, R., et al. 2007a, The Astronomer's Telegram, 1034, 1
Masetti, N., Landi, R., Pretorius, M. L., et al. 2007b, A&A, 470, 331
Miyaji, T., & Boldt, E. 1990, ApJ, 353, L3
Molkov, S., Mowlavi, N., Goldwurm, A., et al. 2003, Astron. Telegram, 176, 1
Molkov, S. V., Cherepashchuk, A. M., Lutovinov, A. A., et al. 2004, Astron. Lett., 30, 534
Morelli, L., Masetti, N., Bassani, L., et al. 2006, Astron. Telegram, 785, 1
Negueruela, I., Smith, D., & Chaty, S. 2005, Astron. Telegram, 470, 1
Negueruela, I., & Smith, D. 2006, Astron. Telegram, 831, 1
Neronov, A., Chernyakova, M., Courvoisier, T. J., & Walter, R. 2005, [arXiv:astro-ph/0506437]
Palmer, D. M., Barthelmey, S. D., Cummings, J. R., et al. 2005, The Astronomer's Telegram, 546, 1
Patel, S., Kouveliotou, C., Tennant, A., et al. 2004, ApJ, 602, L45
Pavlinskii, M. N., Grebenev, S. A., & Syunyaev, R. A. 1992, Sov. Astron. Lett., 18, 88
Pfeffermann, E., & Aschenbach, B. 1996, Roentgenstrahlung from the Universe, 267
Plionis, M., & Kolokotronis, V. 1998, ApJ, 500, 1
Produit, N., Ballet, J., & Mowlavi, N. 2004, The Astronomer's Telegram, 278, 1
Protheroe, R. J., Wolfendale, A. W., & Wdowczyk, J. 1980, MNRAS, 192, 445
Rea, N., Testa, V., Israel, G., et al. 2006, Astron. Telegram, 713, 1
Rees, M. J. 1980, IAUS, 92, 207
Reig, P., Negueruela, I., Papamastorakis, G., Manousakis, A., & Kougentakis, T. 2005, A&A, 440, 637
Renaud, M., Gros, A., Lebrun, F., et al. 2006a, A&A, 456, 389
Renaud, M., Bélanger, G., Paul, J., Lebrun, F., & Terrier, R. 2006b, A&A, 453, L5
Revnivtsev, M. G., Sazonov, S. Y., Gilfanov, M. R., & Sunyaev, R. A. 2003a, Astron. Lett., 29, 587
Revnivtsev, M., Tuerler, M., Del Santo, M., et al. 2003b, IAUC, 8097, 1
Revnivtsev, M., Chernyakova, M., Capitanio, F., et al. 2003c, Astron. Telegram, 132, 1
Revnivtsev, M., Sazonov, S., Jahoda, K., & Gilfanov, M. 2004a, A&A, 418, 927
Revnivtsev, M., Sazonov, S., Churazov, E., et al. 2004b, A&A, 425, L49
Revnivtsev, M., Sunyaev, R., Varshalovich, D., et al. 2004c, Astron. Lett., 30, 382
Revnivtsev, M. G., Sunyaev, R. A., Gilfanov, M. R., et al. 2004d, Astron. Lett., 30, 527
Revnivtsev, M. G., Sazonov, S. Y., Molkov, S. V., et al. 2006, Astron. Lett., 32, 145
Richstone, D., Ajhar, E. A., Bender, R., et al. 1998, Nature, 395, A14
Rodriguez, J., Domingo Garau, A., Grebenev, S., et al. 2004, Astron. Telegram, 340, 1
Rodriguez, J., Cabanac, C., Hannikainen, D. C., et al. 2005, A&A, 432, 235
Rowan-Robinson, M., Sharpe, J., Oliver, S. J., et al. 2000, MNRAS, 314, 375
Saunders, W., Sutherland, W. J., Maddox, S. J., et al. 2000, MNRAS, 317, 55
Sazonov, S., Churazov, E., Revnivtsev, M., Vikhlinin, A., & Sunyaev, R. 2005, A&A, 444, L37
Sazonov, S., Revnivtsev, M., Krivonos, R., Churazov, E., & Sunyaev, R. 2006, A&A, 462, 57
Sguera, V., Bazzano, A., Bird, A., et al. 2006, ApJ, 646, 452
Sguera, V., Hill, A. B., Bird, A. J., et al. 2007, A&A, 467, 249
Skinner, G. K., Ponman, T. J., Hammersley, A. P., & Eyles, C. J. 1987, Astroph.Sp.Sci., 136, 337
Smith, D. M., Heindl, W. A., Markwardt, C. B., et al. 2006, ApJ, 638, 974
Slane, P., Gaensler, B. M., Dame, T. M., et al. 1999, ApJ, 525, 357
Sunyaev, R., Lutovinov, A., Molkov, S., & Deluit, S. 2003a, Astron. Telegram, 181, 1
Sunyaev, R. A., Grebenev, S. A., Lutovinov, A. A., et al. 2003b, The Astronomer's Telegram, 190, 1
Tonry, J. L., Blakeslee, J. P., Ajhar, E. A., & Dressler, A. 2000, ApJ, 530, 625
Tomsick, J., Lingenfelter, R., Walter, R., et al. 2003, IAUC, 8076, 1
Tomsick, J., Lingenfelter, R., Corbel, S., Goldwurm, A., & Kaaret, P. 2004, Astron. Telegram, 224, 1
Tomsick, J., Chaty, S., Rodriguez, J., et al. 2006, ApJ, 647, 1309
Toor, A., & Seward, F. D. 1974, AJ, 79, 995
Torres, M. A. P., Steeghs, D., Garcia, M. R., et al. 2005, Astron. Telegram, 551, 1
Tueller, J., Barthelmy, S., Burrows, D., et al. 2005, Astron. Telegram, 669, 1
Turler, M., Bel, M. C., Diehl, R., et al. 2005, Astron. Telegram, 624, 1
Ubertini, P., Lebrun, F., Di Cocco, G., et al. 2003, A&A, 411, L131
Ubertini, P., Bassani, L., Malizia, A., et al. 2005, ApJ, 629, L109
Walter, R., et al. 2004, Astron. Telegram, 229, 1
Walter, R., Zurita Heras, J., Bassani, L., et al. 2006, A&A, 453, 133
Winkler, C., Courvoisier, T., Di Cocco, G., et al. 2003, A&A, 411, L1